PRAMANA — journal of physics

Vol. 76, No. 4
April 2011
pp. 573–589

Investigation of Δ(3,3) resonance effects on the properties of neutron-rich double magic spherical finite nucleus, ^{132}Sn, in the ground state and under compression

MOHAMMED H E ABU-SEI'LEEK
Department of Physics, Al-Jouf University, Skaka, Saudi Arabia
E-mail: moh2hassen@yahoo.com

MS received 6 May 2010; revised 2 December 2010; accepted 18 October 2010

Abstract. Within the framework of the radially constrained spherical Hartree–Fock (CSHF) approximation, the resonance effects of delta on the properties of neutron-rich double magic spherical nucleus ^{132}Sn were studied. It was found that most of the increase in the nuclear energy generated under compression was used to create massive Δ particles. For ^{132}Sn nucleus under compression at 3.19 times density of the normal nuclear density, the excited nucleons to Δs were increased sharply up to 16% of the total number of constituents. This result is consistent with the values extracted from relativistic heavy-ion collisions. The single particle energy levels were calculated and their behaviours under compression were examined. A meaningful agreement was obtained between the results with effective Hamiltonian and that with the phenomenological shell model for the low-lying single-particle spectra. The results suggest considerable reduction in compressibility for the nucleus, and softening of the equation of state with the inclusion of Δs in the nuclear dynamics.

Keywords. Nuclear structure; compressed finite nuclei; Δ-resonance.

PACS Nos 21.60.Cs; 21.60.Jz; 24.30.Gd

1. Introduction

The Δ resonance degree of freedom plays an important role in nuclear physics, such as the nucleon–nucleon scattering, nuclear structure, heavy-ion collisions and so on. Nuclei are expected to be compressed during high-energy heavy-ion collisions [1]. The issue of compressed nuclei is important in astrophysics and so this issue cannot be ignored. Their experimental as well as theoretical investigations are intricate in particular, because the compressed state is hard to realize statically. The theoretical analyses of heavy-ion collisions consequently start from kinetic equations. Nuclei are not infinitely extended and have no stabilizing crystalline background as solids, which can be assumed in band structure calculations of solids. The structure of nuclei with their finite number of particles

has to be calculated from extensive many-body problems or by simulating an effective nucleon–nucleon (N–N) interaction and transition potentials which are not well known.

One of the most fundamental and elusive problems in theoretical nuclear physics is to understand the structure of finite nuclei in terms of the N–N interaction [2]. In conventional nonrelativistic microscopic structure calculations, the nucleus is considered as a composite system of elementary particles (protons and neutrons) with no internal degree of freedom. With the advent of high precision experiments at intermediate and high energies using a variety of probes, the contribution of baryon resonances to the structure of nuclei in their ground state and under compression becomes a major experimental and theoretical question [3,4]. For example, some relativistic heavy-ion collision data show that as much as 10% of the nuclear system can be excited into Δ resonances [5–7]. Nucleons are no longer treated as elementary or structureless particles, and the internal dynamics of nucleons has to be taken into consideration. One method that incorporates the dynamics associated with the structure of the nucleons in the nuclear system is to consider the excitation of the nucleon into Δ isobars. This excitation can occur as a result of an external static load on the nucleus [8]. The excitation of Δ isobars is very important to understand the structure of nuclei at intermediate and high energies. It forms various probes to provide an exciting challenge both theoretically and experimentally, especially in the search for constructive, coherent pion production [9,10]. The Δ excitation and its decay to nucleon and pion are of current interest in understanding the collision of light and heavy ions [11–16].

Investigating the delta formation in the nucleus as a function of compression is very important to understand heavy-ion collision [17], and astrophysical environments of interest such as supernova explosions or structure of neutron stars [18] which are very important in these days in supercolliders when two energetic heavy ions collide. The predictions for highly compressed nuclei at densities accessible to relative heavy-ion collisions are made.

The Δ isobar is an important mode of nucleonic excitation. It is due to a resonance in pion–nucleon scattering, photopion and electropion production from nucleon. In nuclear structure, the Δ resonance is an agent for corrections in the traditional picture of the nucleus as a system of nucleons only [19,20], and so it is considered as a nucleus constituent, beside nucleons. The Δ isobar provides a mechanism for pion scattering, pion production and pion absorption [21].

Within the framework of CSHF approximation, in the present work, the Δ resonance effects on the properties of the neutron-rich double magic spherical nucleus, ^{132}Sn, including its ground state and the state under static compression were studied. Heavy nuclei with a large neutron excess develop a neutron skin which is an outer coat of neutron-rich nuclear matter around the core [22]. The region of nuclei around doubly-magic ^{132}Sn is currently a subject of theoretical and experimental interest [23]. The physical interest of Δ resonances is useful for the investigation of the equation of state of dense nuclear matter at high densities, where the Δ degree of freedom may appear. This is also a hot topic of the current heavy-ion physics research and compact star physics [24]. Calculations were performed using CSHF approximation with a model space of six major oscillator shells and a realistic effective Hamiltonian [25] with N–N, N–Δ and Δ–Δ interactions. The effective baryon–baryon interaction was evaluated using the Brueckner G-matrix [23,26–31], and its adopted improvement [8,32,33].

The theory of effective operators plays an important role in the modern approach to nuclear structure. Effective interaction is the basic ingredient of the no-core shell model,

one of the methods that provides a solution to the nuclear many-body problem starting from N–N and N–Δ interactions. Numerical solution to the A-body Schrödinger equation can be obtained only if one truncates the Hilbert space to a finite space, yet of sufficiently small dimension. Restriction of the space to a numerically tractable size requires that operators for physical observables be replaced by effective operators that are designed to account for such effects [34].

The results of the role of Δs in finite nuclei have been investigated [8,31–33,35–44]. The nucleus has been considered as a collection of nucleons and Δ-resonances. The effects of including the Δ degrees of freedom on the Hartree–Fock energy, density distribution, Δ-orbital occupations and single-particle energies in the ground state and under low-amplitude static compression, have been examined in model space consisting of seven major oscillator shells. The selected nuclei are: ^{16}O, ^{40}Ca, ^{56}Ni, ^{90}Zr, ^{100}Sn and ^{132}Sn.

In this work, these effects were examined in heavy neutron-rich double magic spherical nucleus ^{132}Sn with a larger amplitude static compression. With an extensive study of nuclear density distributions, different model spaces consisting of six major oscillator shells with the CSHF approximation were used as a realistic effective Hamiltonian with different potentials. The Bruekner G-matrices were used which were generated from coupled channels NN, NΔ and πNN [23,25–29]. This is done to give a clear description of NN data up to 1 GeV. The method for calculating the effective interactions of the nuclear shell model [23,45] was used in this work. It is a good tool to study the highly compressed nuclei at densities accessible to relativistic heavy-ion collisions.

The paper is organized as follows. Section 2 specifies the effective Hamiltonian and the model space used in the calculation. The procedure and strategy are outlined in §3. Results and discussions are presented in §4 and conclusions are presented in §5.

2. Effective Hamitionian H_{eff} and model space

For a nuclear system of Δ baryons, mass, spin and isospin of the nucleon are m, $1/2$ and $1/2$, respectively. For Δ baryon, the mass, spin and isospin are M, $3/2$ and $3/2$, respectively. The intrinsic mass operator Hamiltonian of this system can be written as

$$H = H_1(\text{one-body}) + H_2(\text{two-body}), \tag{1}$$

where

$$H_1(\text{one-body}) = \left[\sum_{i=1}^{A} \frac{p_i^2}{2M}\left(\frac{m-M}{m}\right) + (M-m)\right]\tau_{\text{op}}^{3/2}, \tag{2}$$

where p_i is the single-particle momentum operator, $\tau_{\text{op}}^{3/2}$ is the single-particle isospin projection operator and A is the mass number. H_1 arises due to the presence of the Δs. It consists of a mass correction and a kinetic energy term for the delta particles multiplied by a factor, which is negative since $M = 1236$ MeV and $m = 939$ MeV. These terms give nonzero contribution in Δ-sector only, as the projection operator $\tau_{\text{op}}^{3/2}$ works in the space $\tau^{3/2}$ only. τ_{op}^{τ} is a single-particle isospin projection operator.

$$\tau_{\text{op}}^{\tau}|\tau'\rangle = \delta_{\tau\tau'}|\tau'\rangle, \tag{3}$$

$$\tau_{\text{op}}^{1/2} + \tau_{\text{op}}^{3/2} = 1. \tag{4}$$

H_2 is the effective baryon–baryon interaction that consists of the effective N–N interaction that is represented by Reid Soft Core (RSC) potential [46] and the transition potentials among baryons, which are given in [47]. It is given by

$$H_2 \text{ (two-body)} = T_{\text{rel}}(m) + V^{\text{BB}'} + V_{\text{C}}, \tag{5}$$

where

$$T_{\text{rel}} = \sum_{i<j} \left(\vec{p}_i - \vec{p}_j\right)^2 / 2mA. \tag{6}$$

T_{rel} is the relative kinetic energy operator. Here, we consider the total mass of the nuclear system as Am, $V^{\text{BB}'}$ is the strong two-baryon interaction operator and V_{C} is the two-particle Coulomb interaction acting between charged baryons.

If the Schrödinger equation is solved in the full infinite Hilbert space of all possible N and Δ many-body configurations, the exact solution has been arrived at, but this is not possible for nuclei with the mass number greater than 16 for which special procedure may be adopted [48–51]. Therefore, the infinite Hilbert space to finite model space is truncated, and an effective Hamiltonian, H_{eff}, to be used in the truncated model space is defined. So, eq. (5) can be written as

$$H_{\text{eff}}(\text{two-body}) = T_{\text{rel}}(m) + V_{\text{eff}}^{\text{BB}'} + V_{\text{C}}. \tag{7}$$

Hence $V^{\text{BB}'}$ in eq. (5) becomes $V_{\text{eff}}^{\text{BB}'}$ that is given by

$$\begin{aligned} V_{\text{eff}}^{\text{BB}'} &= V_{\text{eff}}^{\text{NN}\leftrightarrow\text{NN}} + V_{\pi,\rho}^{\text{NN}\leftrightarrow\text{N}\Delta} + V_{\pi,\rho}^{\text{NN}\leftrightarrow\Delta\Delta} + V_{\pi,\rho}^{\text{N}\Delta\leftrightarrow\text{N}\Delta} \\ &\quad + V_{\pi,\rho}^{\text{N}\Delta\leftrightarrow\Delta\text{N}} + V_{\pi,\rho}^{\text{N}\Delta\leftrightarrow\Delta\Delta} + V_{\pi,\rho}^{\Delta\Delta\leftrightarrow\Delta\Delta}. \end{aligned} \tag{8}$$

The Coulomb term, V_{C}, is taken to be the average Coulomb potential energy per proton and Δ^+ in a uniformly charged sphere

$$V_{\text{C}} = \frac{6}{5}\frac{Ze^2}{R}\left[1 - 5\left(\frac{3}{16\pi Z}\right)^{2/3} - \frac{1}{Z}\right], \tag{9}$$

where the $Z^{2/3}$ term is the exchange contribution and the Z^{-1} term subtracts the interaction of the proton with itself and Δ^+.

By applying the variation principle, the Hartree–Fock equation for nucleon and delta orbitals can be derived which can be used as the effective Hamiltonian within the chosen model space. Compression is achieved by applying a static load. The radial constraint acts like an external force to compress or expand the nucleus (see [35–41]).

In calculations, no-core oscillator model space having six major oscillator shells was used. In the 5-space (6 shells), 21 nucleon orbitals were used:

$$\begin{aligned} &0s_{1/2}, 0p_{3/2}, 0p_{1/2}, \ 0d_{5/2}, 1s_{1/2}, 0d_{3/2}, 0f_{7/2}, 1p_{3/2}, 0f_{5/2}, 1p_{1/2}, 0g_{9/2}, 1g_{7/2}, \\ &1d_{5/2}, 1d_{3/2}, 2s_{1/2}, 0h_{11/2}, 0h_{9/2}, 1f_{7/2}, 1f_{5/2,}2p_{3/2}, 2p_{1/2}, \end{aligned}$$

and for delta states, six delta orbitals were used:

$$0s_{3/2}, 0p_{3/2}, 0p_{1/2}, 1s_{3/2}, 1p_{3/2}, 1p_{1/2}.$$

A total of 27 baryon orbitals were included. Since $0s_{3/2}$, $1s_{3/2}$, $0p_{5/2}$, $1p_{5/2}$, $0d_{7/2}$ and $0f_{9/2}$ do not contribute and do not preserve the total angular momentum and isospin symmetry,

these delta orbitals were not used. Only a few of them were taken into account because of the lack of access to supercomputers and large parallel computing machines. Therefore, the current numerical calculation was done by personal computers only.

A no-core model space having six major shells was chosen to avoid calculating the core polarization effects with realistic effective interaction. In addition, all nucleons were active, and hence there were no terms in the $V_{\text{eff}}^{\text{BB}'}$ expansion involving particle–hole excitations.

The matrix elements of the effective Hamiltonian was calculated using the Brueckner G-matrix method [23,25]. The effective N–N interaction was the sum of the Brueckner G-matrix and the lowest order fold diagram acting between pairs of nucleons in a no-core model space [51–53]. RSC potential for the N–N interaction was adopted.

The parameters of the interaction are mostly determined for nuclei at their ground-state density. The Hartree–Fock calculations here extend up to more than three times of this density using the same interaction. In the previous work [35–41], the effective NN $\leftrightarrow$ NN interaction was calculated from a G-matrix approach [54,55], while the baryon–baryon effective interactions associated with the Δ were taken from a potential model. Therefore, the Brueckner-type [56,57] NΔ correlation was not included in the calculations. This deficiency is removed in the present work by using the method developed in [45] to define Δ effective interaction from G-matrix element. These G-matrix elements were generated from a coupled-channel NN $\oplus$ NΔ $\oplus$ πNN model [26–31], which was constrained by the data of both the NN elastic scattering and the NN $\rightarrow$ NΔ $\rightarrow$ πNN reaction. Therefore, the strength for the NN $\rightarrow$ NΔ transition, a crucial element in predicting Δ components in nuclei, is more under control than that of the potential model [56,57] used in [35–41]. These improvements are important for investigating a compressed nuclear system with large density in which the high momentum components of the effective interaction play an important role [32,33].

It is convenient to view the nuclear effective two-body part Hamiltonian matrix element in the harmonic oscillator single-particle basis in the following schematic diagram:

$$\left(\begin{array}{l|l} \text{Pure N–N sector} & \text{N–}\Delta\text{ sector} \\ \langle V_{\text{eff}}^{\text{NN}}\rangle + \langle T_{\text{rel}}\,(m)\rangle + \langle V_{\text{C}}^{\text{pp}}\rangle & \langle V_{\text{eff}}^{\text{N}\Delta}\rangle + \langle V_{\text{C}}^{p\Delta^+}\rangle \\ \hline \Delta\text{–N sector} & \text{Pure }\Delta\text{–}\Delta\text{sector} \\ \langle V_{\text{eff}}^{\Delta\text{N}}\rangle + \langle V_{\text{C}}^{\Delta^+ p}\rangle & \langle H_1\,(\text{one-body})\rangle + \langle V_{\text{eff}}^{\Delta\Delta}\rangle \\ & + \langle T_{\text{rel}}\,(m)\rangle + \langle V_{\text{C}}^{\Delta^+\Delta^+}\rangle \end{array}\right) = \langle H_2\,(\text{two-body})\rangle.$$

Nucleons to be excited to Δs from N–N sector were allowed. The description of the model space which was used in this study was completed.

3. Calculation procedure and strategy

The strategy used is the same as in [41–44] and is summarized as follows: (1) the effective Hamiltonian in the nucleon sector only is considered (i.e. by turning off N–Δ interaction). This is followed by calculating the ground state properties in the spherical Hartree–Fock approximation (i.e. Hartree–Fock energy, $E_{\rm HF}$, and the root mean square radius, $r_{\rm rms}$) by adjusting the strength of the kinetic and potential factors in $H_{\rm eff}$ until an agreement is reached between spherical Hartree–Fock results and the experimental binding energy and experimental radius at equilibrium. The adjusting parameters λ_1 and λ_2 are introduced to adjust the matrix elements of $T_{\rm ref}$ and $V_{\rm eff}$, respectively. As the two-body matrix elements are evaluated with an oscillator energy spacing $\hbar\omega = 14$ MeV, these matrix elements are scaled to the new oscillator basis characterized by new value of $\hbar\omega'$ as described in [52,53,58]. (2) the N–Δ and Δ–N interactions are activated. The adjusting parameters and $\hbar\omega'$ for ^{132}Sn nucleus in a given model space at equilibrium with the Δ channel turned off are obtained in table 1. (3) the N–Δ and Δ–N interactions are turned off and a radial constraint, $-\beta r^2$, is utilized to include static compression, where r is the one-body scalar radius operator. (4) the N–Δ and Δ–N interactions are activated and the radial constraint, $-\beta r^2$, is applied and the difference in $E_{\rm HF}$ from the third step and current step as a function of $r_{\rm rms}$ is observed.

The computations of this work were done by three major steps, the outline of which is presented below.

Step 1: The relative centre of mass matrix elements of the transition potentials $V^{\rm N\Delta}$ and $V^{\rm \Delta N}$ [34,35] was evaluated using a computer program developed for this purpose. The output of the program was the matrix elements in a format suitable for the second step of the calculations. The limits on the relative quantum numbers $n, n', \ell, \ell', s, s'$, and the total isospin τ were all taken up to 3. The limit on the relative total angular momentum g was taken up to 6. The change in the orbital angular momentum ($\Delta\ell$) and spin (Δs), were 0 and ± 2, respectively.

Step 2: Another computer program was developed to evaluate the two-body matrix elements of the transition potentials in two-particle basis coupled with a good total angular momentum, J, and total isospin, τ. The two-particle basis was constructed from a harmonic oscillator single-particle state (nucleon orbitals and Δ-orbitals), which was characterized by the quantum numbers $n,\ \ell,\ s,\ j,\ \tau$. The relative centre of mass transition matrix elements calculated in Step 1 were read in, and each matrix element underwent a set of tests to show whether it was required by the constructed two-particle states. If it passed all the

Table 1. Adjusting parameters λ_1, λ_2 and $\hbar\omega'$ of the effective Hamiltonian for ^{132}Sn for the model space of six oscillator shells for which the calculations were performed. The binding energy (point mass $r_{\rm rms}$) that was fitted was -1104 MeV (5.63 fm) for ^{132}Sn.

Nucleus	λ_1	λ_2	$\hbar\omega'$ (MeV)
^{132}Sn	0.993	1.370	5.513

tests, then it was stored with an identifying code number. These matrix elements would be multiplied by the appropriate transformation coefficients. The calculations for these steps were based on eq. (13) in [36]. The matrix elements were evaluated in a no-core model space consisting of six major oscillator shells (i.e. 21 nucleon orbitals) and six Δ-orbitals. The output of this program was served was an input for Step 3, i.e. the constraint spherical Hartree–Fock calculations.

Step 3: A spherical Hartree–Fock computer program was developed to calculate this phase according to eqs (33) and (34) in [36]. The main processes in one iteration of CSHF calculations is outlined as follows: the information about the number of particles, number of single-particle states, number of Hartree–Fock occupied states and their $2j$ values, the $2j$ and n values of the harmonic oscillator orbitals $\hbar\omega$, $\hbar\omega'$, and the number of iterations were read and stored.

The first quantities to be calculated and stored were the Hartree–Fock Hamiltonian matrix elements $\langle B|H|B'\rangle$ according to eq. (33) in [36]. For this, baryon densities of value unity were read and stored. The appropriate two-body matrix elements of the effective Hamiltonian, which were precalculated and stored in Stage 2, were retrieved. The computer code was designed, such that, if it encountered a two-body matrix elements in the N–N sector, it retrieved previous calculated G-matrix elements, the kinetic energy ($T_{\rm rel}$), matrix elements and the Coulomb energy matrix elements were scaled as mentioned before. A set of Hartree–Fock Hamiltonian matrix elements was used to calculate a second set of Hartree–Fock matrix element $\langle B|H|B'\rangle'$, which includes the constraint term and is defined by

$$\langle B|H|B'\rangle' = \langle B|H|B'\rangle - \beta\langle B|r^2|B'\rangle. \tag{10}$$

This second set of Hartree–Fock Hamiltonian matrix elements was used to calculate the corresponding eigenvalues and eigenvectors. The eigenvectors in turn were used to calculate new baryon densities and the number of Δ-particles in the occupied orbitals. The new baryon densities were used to calculate the root mean square radius $r_{\rm rms}$.

Finally, the Hartree–Fock energy, $E_{\rm HF}$, was calculated according to eq. (34) in [36]. This was the end of the first iteration. The second iteration started with the baryon densities calculated in the first iteration and proceeded as the first iteration to calculate the described quantities. The self-consistent process continued until a convergent solution was achieved.

4. Results and discussions

In [33,38,39], some selected results for ^{132}Sn demonstrating the behaviour of self-consistent single-particle spectra as a function of compression were presented. In the present work, more detailed results for ^{132}Sn are presented in order to examine its properties under static compression. The N–Δ and Δ–Δ interactions were employed as they were activated in a model space consisting of six major oscillator shells (excluding $\ell > 5$) for nucleons and six orbitals for Δs making a total of 27 baryons orbitals.

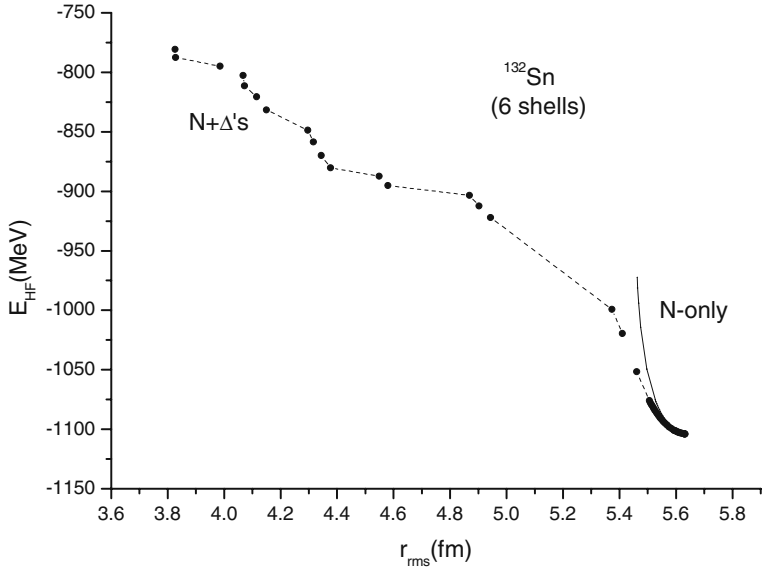

Figure 1. CSHF energy as a function of the point mass $r_{\rm rms}$ using RSC potential for ^{132}Sn evaluated for six major oscillator shells with six Δ-orbitals. The dashed curve corresponds to CSHF with full calculations including the Δs whereas the solid curve corresponds to CSHF with nucleons only.

The equilibrium point is at a point mass radius 5.63 fm, which is given with other properties in table 1 and in all the figures. The calculations were performed for ^{132}Sn. The Hartree–Fock energies, $E_{\rm HF}$, vs. $r_{\rm rms}$ using RSC potential are displayed in figure 1, which clearly shows that there is virtually no difference in the results with or without Δs at equilibrium. It is seen that without the Δ degree of freedom in the system, $E_{\rm HF}$ increases steeply towards zero binding energy under compression. As the volume of the nucleus decreases by about 9%, the binding energy will be about 46.27 MeV, when Δ-excitations are included in the results obtained when only the nucleons are considered. That is, it shows about 131.60 MeV and 85.33 MeV of excitation energy to achieve a 9% volume reduction in the nucleon-only results, and nucleons and Δ^+s results, respectively.

As shown in the above results, it costs 85.33 MeV of excitation energy to reduce the volume by 9% and to reduce the energy by 8% more. This suggests that the less dense outer part of the nucleus initially responds to the external load more readily than the inner part.

It can be seen from figure 1 that 323.32 MeV of excitation energy is needed to achieve a 69% volume reduction when the Δ degree of freedom is included in the system. Most of this energy is used to create massive Δ particles.

The difference between the results of the Hartree–Fock binding energy obtained in previous studies [33,38,39] and the results in this work is the size of the nucleon model space, the number of the Δ orbitals included, different potentials, and more compression. Also, it is worth mentioning that at equilibrium (no constraint) in ^{132}Sn, no mixing between

nucleon states and the Δ states was found. As in [33,38,39], all curves of E_{HF} agree near the equilibrium ($r_{\mathrm{rms}} = 5.63$ fm). This implies that results for the system at equilibrium do not depend on model space. In comparison with results in [33,38,39], current results are consistent with those obtained for ^{132}Sn for E_{HF} with different model spaces, but the curve of N-only is very steep. This is due to the smallest model space, so the static compression modulus is increased significantly by the reduced nucleon model space. The current results show more compression than the previous studies. The results show that there is a significant reduction in the static compression modulus for RSC static compressions which is reduced by including the Δ excitations. The consequence of this reduction is the softening of the nuclear equation of state at larger compressions.

It is shown from figure 1, that as the static load force increases, the compression of nucleus with only nucleons is less than the other nucleus with nucleons and Δs.

One potential consequence of this result is that it could represent a collective mechanism for 'sub-threshold' pion production. That is, in 'sub-threshold' pion production experiments between the colliding nuclei, if the collision produces isothermal compression, then the Δs are populated and relaxation can occur by the decay of Δ to a nucleon and a pion.

Figure 2 gives an impression of the role of the Δs as a function of compression – the number of Δs against r_{rms}. The total number of Δs and the number of Δ^+s and Δ^0s are plotted separately.

In figure 2, it can be seen that the deltas increase rapidly as volume decreases. When the nucleus volume is reduced to about 69% of its volume at equilibrium, the number of deltas is increased to about 16% of all constituents of ^{132}Sn. It is interesting to note in figure 2 that the number of Δ^0s and Δ^+s are different at increased compression. The creation of Δ^0s becomes more favourable as the compression continues because the number of neutrons is

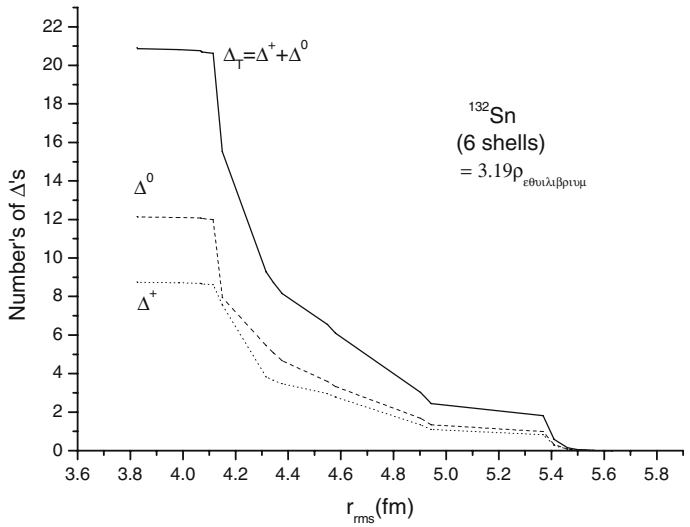

Figure 2. Number of Δs as a function of r_{rms} for ^{132}Sn in six major shell model spaces. The upper curve indicates the total number of Δs, the dotted curve indicates the number of Δ^+, and the dashed curve indicates Δ^0.

greater than the number of protons. When 21 Δs are presented, the excitation energy values are around $21(M - m) \approx 6237$ MeV. Thus, on the scale of the unperturbed single-particle energies, a substantial fraction of the compressive energy is delivered, through N–Δ and Δ–N interactions, to create more massive baryons in the lowest energy configuration of the nucleus. In other words, the number of Δs can be increased to about 21 at $r_{\rm rms} = 3.83$ fm which corresponds to about 3.19 times the normal density.

It can be seen from figure 2 that the number of Δs is increased until $r_{\rm rms} = 4.1$ fm, but beyond this radius, the number of Δs become constant. The number of Δ^0 is greater than the number of Δ^+ by about 75% at this radius and this difference remains constant during compression. This effect occurs because converted rate from nucleon states to Δ states becomes constant in this case. This major difference from the previous studies [33,38,39] is because of the compression.

In other words, figure 2 shows that the number of Δs formed increases sharply, when ^{132}Sn nucleus is compressed to a volume of about 0.69 of its equilibrium size. However, at this nuclear density, which is about three times the normal density, the percentage of nucleons converted to Δ is only about 16% in ^{132}Sn.

Comparing the results in figure 10 of [33], figure 3 of [38] and figure 4 of [39] with the present results in figure 2, the number of Δs increases as the model space decreases. From figure 10 in [33], the formation of Δs becomes more favourable as the compression continues as model space decreases. The present results show a major difference from other findings [33,38,39].

Figure 2 exhibits sudden changes in curvature of the Δ-population curves. The curves for Δ^0 and Δ^+ become flat from $r = 4.1$ fm to 3.8 fm. These abrupt features may be artifacts of the small number of Δ orbitals employed, and may be due to the small gap between the $n = 0$ and $n = 1$ Δ-single particle energies. As moving to larger compression, the Δ states reduce the static compression modulus, but their role in reducing the static modulus is less dramatic than enlarging the size of the nucleon model space. The role of Δ states in reducing the static compression modulus is the largest in the smallest space.

In terms of the relativistic heavy-ion collisions, the nucleus that can more easily penetrate, when the Δ degree of freedom becomes explicit, is implied by figure 1. Because of the limitations of the model space, the calculations for higher densities are more speculative. Nevertheless, it can give us some idea about how the Δ population can be increased as the nucleus is compressed to higher densities accessible to relativistic heavy-ion collisions. The results shown in figures 1 and 2 are consistent with the results extracted from relativistic heavy-ion collisions [59–61].

The formation of Δ^0s becomes more favourable when the compression continues than when model space decreases. Figure 3 displays the radial density distribution for ^{132}Sn at large compression and point mass radius $r_{\rm rms} = 5.37$ fm in a model space of six major oscillator shells with Δ excitation restricted to the six orbitals: $0s_{3/2}$, $0p_{1/2}$, $0p_{3/2}$, $1s_{3/2}$, $1p_{1/2}$, $1p_{3/2}$. The radial density distributions for neutrons $\rho_{\rm n}$, protons $\rho_{\rm p}$, deltas ρ_Δ, and their sum $\rho_{\rm T}$ as a function of the radial distance from the centre of the nucleus at large compression in five oscillator model spaces are shown in figure 3. Moreover, the neutron radial density is higher than the proton density at all values of r because of the Coulomb repulsion between the protons. Even though the Δ-density appears to be zero at equilibrium, the Δ-radial density distribution, under high compression (point mass $r_{\rm rms} = 5.37$ fm), reaches a peak value of about 0.38 of the proton radial density at

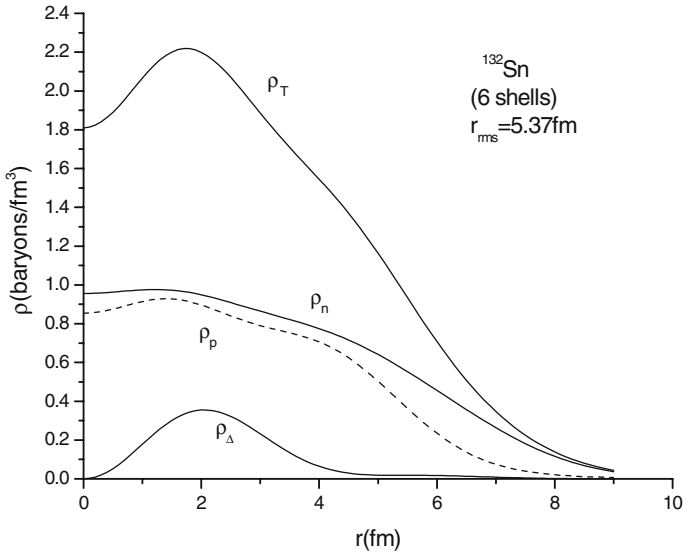

Figure 3. Total ρ_{T}, proton ρ_{p} (dashed line), neutron ρ_{n} (solid line) and delta ρ_{Δ} radial density distributions for ^{132}Sn at $r_{\mathrm{rms}} = 5.37$ fm in a model space of six major oscillator shells.

$r = 2$ fm. Δ-mixing with the nucleons in the $0p_{1/2}$, $0p_{3/2}$, $1p_{1/2}$ and $1p_{3/2}$ orbitals occurs, which explains the shape of the Δ-radial distribution presented in figure 3.

Figure 4 displays the radial density distributions of ^{132}Sn evaluated at about 0.47 reduced volume ($r_{\mathrm{rms}} = 4.38$ fm). In this case, the Δ-radial density distribution reaches a peak value of about 2.89 of the proton radial density.

In figures 3 and 4, the radial density distribution for Δ reaches zero at the origin since the number of Δ increases as compression increases at the expense of the number of nucleons. Therefore, the radial density distribution of Δ increases at the expense of the radial density distribution of nucleons when compression increases. This explains the radial density distribution of Δ, in figure 5, not reaching zero but approaching the value of proton and neutron at higher compression.

Figure 5 shows that the Δ-radial density distribution reaches a peak value of about 3.55 of the proton radial density of ^{132}Sn evaluated at higher compression at about 0.31 reduced volume ($r_{\mathrm{rms}} = 3.83$ fm).

It can be seen from figures 3–5 that as compression increases the total radial density increases and the radial density distribution of Δs increases sharply, but radial density of nucleons decreases sharply. If these results are substantial, they could have interesting consequences for sub-threshold pion production experiments in nucleus–nucleus collisions where the bombarding energy per nucleon is below that needed to produce pions in free N–N collisions. To the extent these collisions produce isothermal compression, relaxation occurs by the decay of Δ to nucleon and pion. These calculations support a collective mechanism for sub-threshold pion production. To our knowledge this mechanism has not been previously explored.

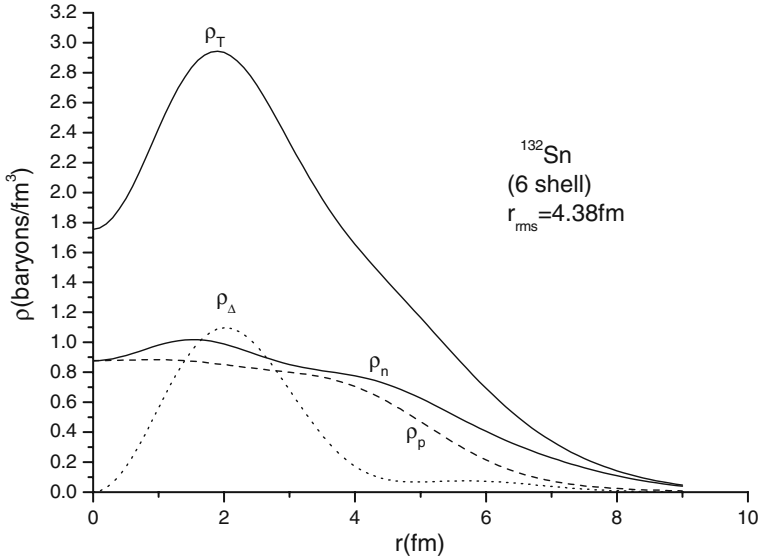

Figure 4. Total ρ_{T}, proton ρ_{p} (dashed line), neutron ρ_{n} (solid line) and delta ρ_{Δ} (dotted line) radial density distributions for ^{132}Sn at $r_{\mathrm{rms}} = 4.38$ fm in a model space of six major oscillator shells.

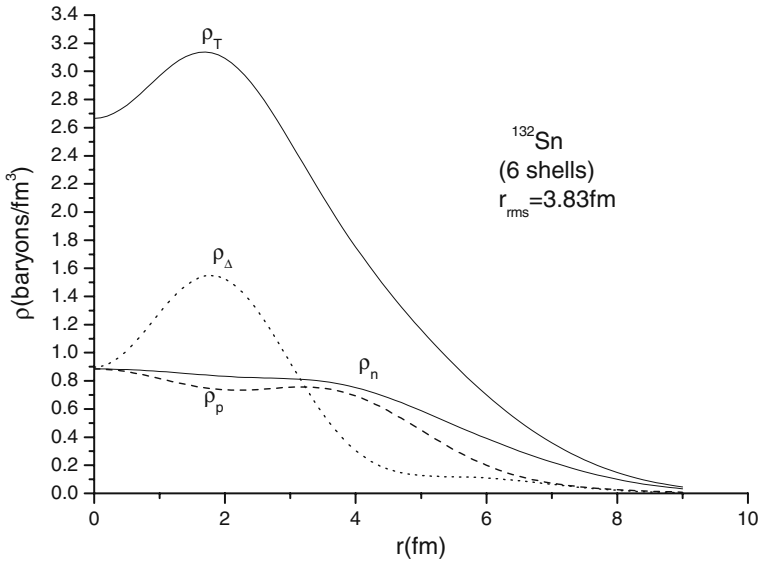

Figure 5. Total ρ_{T}, proton ρ_{p} (dashed line), neutron ρ_{n} (solid line) and delta ρ_{Δ} (dotted line) radial density distributions for ^{132}Sn at $r_{\mathrm{rms}} = 3.83$ fm in a model space of six major oscillator shells.

Figure 6 shows the total radial density for ^{132}Sn in six oscillator shells at large compression ($r_{\rm rms} = 5.37$ fm) and at equilibrium (point mass radius $r_{\rm rms} = 5.63$ fm). The volume of the nucleus is decreased by 0.13 of the equilibrium volume and the radial density is increased by 1.15 of its value at equilibrium.

The results for the matter distribution of ^{132}Sn ground state are also shown in figure 6. For the nucleon distribution, the results are very close to that from the calculation of figure 11 in [33] with different model spaces.

Clearly, the interior density rises relative to the interior density at equilibrium as the nucleus is compressed. This is contrary to the radial density on the outer surface, where the radial density distribution is higher at equilibrium than when the static load is applied.

In figure 7, the lowest self-consistent zero-change single-particle energy levels as a function of $r_{\rm rms}$ are displayed. The orbits curve up as the load on the nucleus increases because the kinetic energy of the baryons which is positive becomes more influential than the attractive mean field of the baryons. The present result is similar to that of figure 1 of [38] with the same model space.

The single-particle energy spectrum also exhibits the gaps between the shells. As the nucleus is compressed, the single-particle level ordering and the gaps are preserved. The general trend is that the single-particle energies (except the deepest bound orbital which actually drops with compression) shift to higher energies as the nucleus is compressed. The curvature goes up more and more as the orbital becomes closer to the surface. This implies that the surface is more responsive to compression than the interior of the nucleus.

It is to be remembered that single-particle spectrum is generated entirely from the underlying microscopic Hamiltonian. Thus, it is remarkable that the calculated spectrum follows

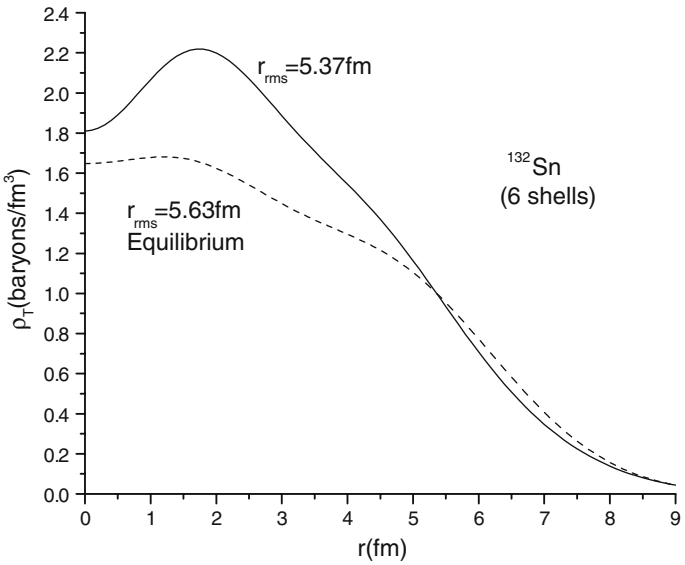

Figure 6. Total radial density distribution for ^{132}Sn at equilibrium ($r_{\rm rms} = 5.63$ fm) (dashed line) and at $r_{\rm rms} = 5.37$ fm (solid line).

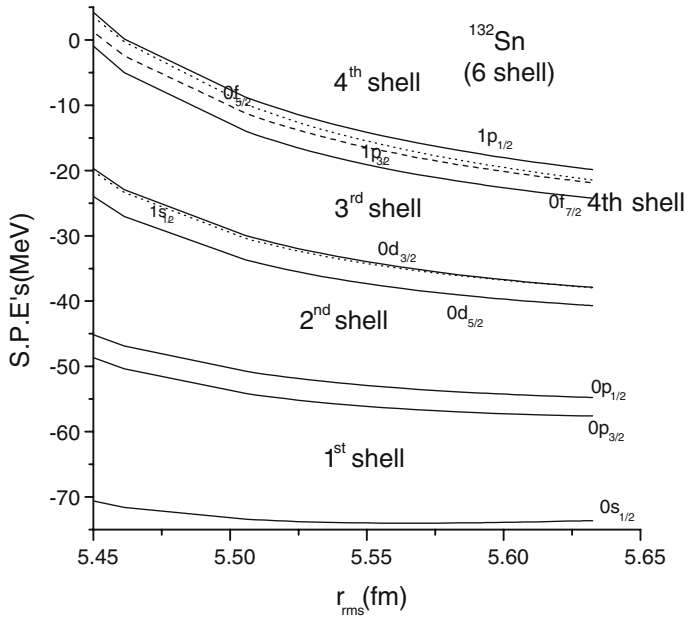

Figure 7. Single-particle energy of the lowest ten neutron states for ^{132}Sn in six oscillator shells as a function of $r_{\rm rms}$.

the expected ordering of the phenomenological shell model in the dominantly nucleon orbitals, and the spectrum exhibits clearly visible gaps between the shells. As the nucleus is compressed, the single-particle level ordering and the gaps are preserved. It is also worth noting that the orbitals which are very close to zero single-particle energy are more sensitive to compression; that means they are more responsive of compression than the interior of the nucleus. The general trend of single-particle energies is to shift to higher energies as the nucleus is compressed.

The behaviour of single-particle energy levels agree well with the orbital ordering of the standard shell model. The gap is very clear between the shells. The splitting of the levels in each shell is an indicator that L-S coupling is strong enough in RSC potential, i.e. L-S coupling becomes stronger as the static load on the nucleus increases. As the nucleus is compressed, the splitting of the orbitals becomes more clear, especially in delta orbitals.

Figure 8 shows the last three unoccupied zero-charge orbitals (lower curves in the figure) and the six orbitals, which are dominantly Δ^0 (higher curves in the figure). Note the gap of about 278.4 MeV between the last dominantly neutron orbital and the first dominantly orbitals because of the difference in rest mass of baryons (neutrons and Δ^0).

The six zero-charge self-consistent single-particle levels which are dominantly Δ^0 in character are displayed in figure 9 as a function of the rms radius. As for the occupied orbitals, there is an expected tendency towards higher energy as the system is compressed. It is interesting to note that the level ordering proceeding from lowest to highest is $0s_{3/2}$, $0p_{1/2}$, $0p_{3/2}$, $1s_{3/2}$, $1p_{1/2}$, $1p_{3/2}$. Although, at some rms radii, some levels approach each other, they do not cross. No clear evidence of shell gaps is found in figure 9.

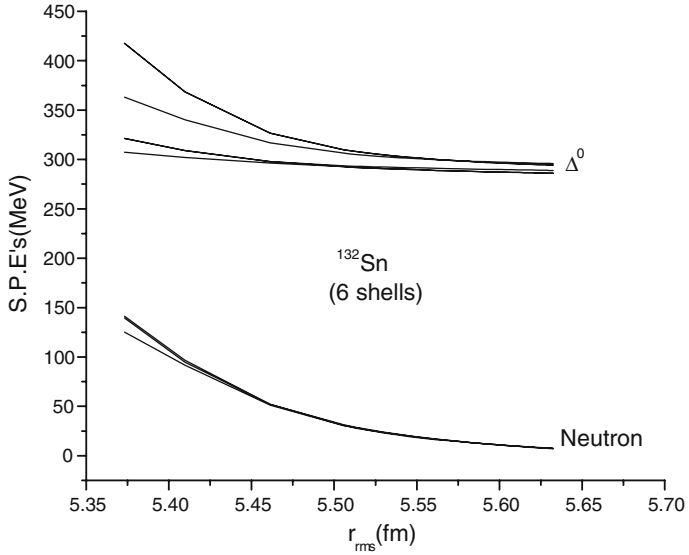

Figure 8. Single-particle energy vs. $r_{\rm rms}$ of the last three unoccupied zero-charge orbitals (low curves) and six orbitals, which are dominantly Δ^0 (higher curves) for ^{132}Sn in model space of six major oscillator shells.

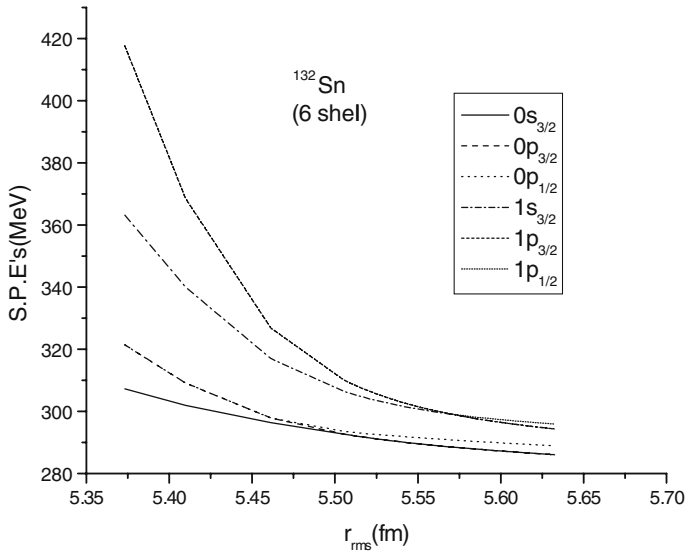

Figure 9. The six dominantly Δ^0 orbitals of ^{132}Sn in six major oscillator shells as a function of $r_{\rm rms}$.

Finally, the behaviour of the positively charged baryon orbitals is not separately presented here as they exhibit properties similar to those of the zero-charge baryons.

5. Conclusions

The ground state properties of ^{132}Sn has been investigated with the Δ degrees of freedom included, using a realistic effective baryon–baryon Hamiltonian within the radial-constrained Hartree–Fock approximation. It can be concluded that the Hartree–Fock energy calculated with a much larger compression decreases as the size of the model space increases for either the N-only or the case including both N and Δ. The Δ excitation of the nucleon is gradually populated as the nucleus is compressed. The nucleus reaches more compressibility when delta particle resonances occur. A more modern potential and the inclusion of Δ resonances together induce a significant softening of the nuclear equation of state for large-amplitude compression. There is considerable reduction of the zero-temperature compressibility when the Δ degree of freedom is activated.

Finally, a large fraction of the excitation energy is required to compress the nucleus used to create mass in the form of Δs. This may have implications for sub-threshold pion production in nucleus–nucleus collisions.

References

[1] T V Chossy and W Stocker, *Phys. Lett.* **B507**, 109 (2001)
[2] J W Negele, *Phys. Rev*. **C1**, 1260 (1970)
[3] E Pasyuk, C Morris, J Ullmann, J Zumbro, L Kwok, J Mathews and Y Tan, *Acta Phys. Pol.* **B29**, 2335 (1998)
[4] C Morris, J Zumbro, J McGill, S Seestrom, R Whitten, C Reidel, A Williams, R Braunstein, M Kohler and B Kriss, *Phys. Lett.* **B419**, 25 (1998)
[5] U Mosel and V Metag, *Nucl. Phys. News* **3**, 25 (1993)
[6] L Xiong, Z Wu, C Ko and J Wu, *Nucl. Phys.* **A512**, 772 (1990)
[7] M Hoffmann *et al*, *Phys. Rev*. **C51**, 2095 (1995)
[8] M A Hasan, T S H Lee and J P Vary, *Phys. Rev*. **C61**, 014301 (1999)
[9] P A Deutchman, *Aust. J. Phys.* **52**, 955 (1999)
[10] C M Terbert *et al*, *Phys. Rev. Lett.* **100**, 132301 (2008)
[11] P Fernández de Córdoba, E Oset and M J Vicente-Vacas, *Nucl. Phys.* **A592**, 472 (1995)
[12] A Badalá *et al*, *Phys. Rev*. **C54**, R2138 (1996)
[13] U Mosel and V Metag, *Nucl. Phys. News* **3**, 25 (1993)
[14] L Xiong, Z G Wu, C M Ko and J Q Wu, *Nucl. Phys.* **A512**, 772 (1990)
[15] M Hoffmann *et al*, *Phys. Rev*. **C51**, 2095 (1995)
[16] X Yong-Zhong, Z Yu-Ming, S Pornrad, Y Yu-Peng and K Chinorat, *Chin. Phys. Lett.* **26**, 022501 (2009)
[17] S Shlomo and V Kolomietz, *Rep. Prog. Phys.* **68**, 1 (2005)
[18] T Frick and H Müther, *Phys. Rev*. **C71**, 014313 (2005)
[19] A M Green, *Rep. Prog. Phys.* **39**, 1109 (1976)
[20] P U Sauer, *Prog. Nucl. Part. Phys.* **16**, 35 (1986)
[21] A Valcare, F Fernánder, H Garcilazo, M T Peña and P U Sauer, *Phys. Rev*. **C49**, 1799 (1996)
[22] A Klimkiewicz *et al*, *Acta Phys. Pol.* **B40**, 589 (2009)
[23] L Coraggio *et al*, *Nucl. Phys.* **A805**, 424c (2008)

[24] S Sarkar and M Sarkar, *Phys. Rev.* **C78**, 024308 (2008)
[25] H B Brandow, *Rev. Mod. Phys.* **39**, 77 (1967)
[26] T Lee, *Phys. Rev. Lett.* **20**, 1571 (1983)
[27] T Lee, *Phys. Rev.* **C29**, 195 (1994)
[28] T Lee and A Matsuyama, *Phys. Rev.* **C32**, 516 (1985)
[29] T Lee and A Matsuyama, *Phys. Rev.* **C36**, 1459 (1987)
[30] A Matsuyama and T Lee, *Phys. Rev.* **C34**, 1900 (1986)
[31] A Matsuyama and T Lee, *Nucl. Phys.* **A526**, 547 (1991)
[32] M A Hasan, T S H Lee and J P Vary, *Phys. Rev.* **C56**, 3063 (1997)
[33] M A Hasan, J P Vary and T S H Lee, *Phys. Rev.* **C64**, 024306 (2001)
[34] B Barrett, I Stetcu, P Navrátil and J Vary, *J. Phys. A: Math. Gen.* **39**, 9983 (2006)
[35] M A Hasan, S H Köhler and J P Vary, *Phys. Rev.* **C36**, 2180 (1987)
[36] M A Hasan, S H Köhler and J P Vary, *Phys. Rev.* **C36**, 2649 (1987)
[37] J P Vary and M A Hasan, *Phys. Rep.* **242**, 139 (1994)
[38] J P Vary and M A Hasan, *Nucl. Phys.* **A570**, 355 (1994)
[39] M A Hasan, *Dirasat J.* **22**, 777 (1995)
[40] M A Hasan and J P Vary, *Phys. Rev.* **C50**, 202 (1994)
[41] M A Hasan and J P Vary, *Phys. Rev.* **C54**, 3035 (1996)
[42] M H Abu-Sei'leek and M A Hasan, *Commun. Theor. Phys.* **54**, 339 (2010)
[43] M H Abu-Sei'leek, *Commun. Theoret. Phys.* **55**, 115 (2011)
[44] M H Abu-Sei'leek, *Nucl. Phys. Rev.* **27**, 399 (2010)
[45] Y Tzeng, T Kuo and T Lee, *Phys. Scr.* **53**, 300 (1996)
[46] R V Reid, *Ann. Phys. (N.Y.)* **50**, 411 (1968)
[47] M Gari, G Niephaus and B Sommer, *Phys. Rev.* **C23**, 504 (1981)
[48] P Navrátil and W Ormand, *Phys. Rev.* **C68**, 034305 (2003)
[49] I Stetcu, B Barrett, P Navrátil and C Johnson, *Int. J. Mod. Phys.* **E14**, 95 (2004)
[50] J Vary *et al*, *Eur. Phys. J.* **A25**, 475 (2005)
[51] M Hasan, J Vary and P Navrátil, *Phys. Rev.* **C69**, 034332 (2004)
[52] G Bozzolo and J Vary, *Phys. Rev. Lett.* **53**, 903 (1984)
[53] G Bozzolo and J Vary, *Phys. Rev.* **C31**, 1909 (1985)
[54] D Zheng, B Barrett, J Vary and R McCarthy, *Phys. Rev.* **C49**, 1999 (1994)
[55] D Zheng, J Vary and B Barrett, *Phys. Rev.* **50**, 2841 (1994)
[56] K Brueckner, *Phys. Rev.* **97**, 1353 (1955)
[57] H Brandow, *Rev. Mod. Phys.* **39**, 771 (1967)
[58] M Saraceno, J P Bozzolo and H G Miller, *Phys. Rev.* **C37**, 1267 (1988)
[59] U Mosol and V Metag, *Nucl. Phys. News* **3**, 25 (1993)
[60] L Xiong and C M Ko, *Nucl. Phys.* **A512**, 772 (1990)
[61] M Hoffmann *et al*, *Phys. Rev.* **C51**, 2095 (1995)